FBXL20 promotes breast cancer malignancy by inhibiting apoptosis through degradation of PUMA and BAX

Rajesh Kumar Manne[1,2], Yashika Agrawal[1,2,‡], Sunil K. Malonia[3,‡], Shahid Banday[3], Sarathkumar Edachery[4], Asha Patel[1], Avinash Kumar[1], Praveenkumar Shetty[4], and Manas Kumar Santra[1,*]

From the [1]Cancer Biology and Epigenetics Laboratory, National Centre for Cell Science, Pune, Maharashtra, India; [2]Department of Biotechnology, S.P. Pune University, Pune, Maharashtra, India; [3]Department of Molecular, Cell and Cancer Biology, University of Massachusetts Medical School, Worcester, Massachusetts, USA; [4]Department of Biochemistry, K. S. Hegde Medical Academy, Nitte University, Mangalore, Karnataka, India

Edited by George DeMartino

Apoptosis is a programmed cell death that efficiently removes damaged cells to maintain tissue homeostasis. Defect in apoptotic machinery can lead to tumor development, progression, and resistance to chemotherapy. PUMA (p53 upregulated modulator of apoptosis) and BAX (BCL2-associated X protein) are among the most well-known inducers of apoptosis. It has been reported that expression levels of BAX and PUMA are controlled at the posttranslational level by phosphorylation. However, the posttranslational regulation of these proapoptotic proteins remains largely unexplored. In this study, using biochemical, molecular biology, flow cytometric, and immunohistochemistry techniques, we show that PUMA and BAX are the direct target of the F-box protein FBXL20, which restricts their cellular levels. FBXL20 directs the proteasomal degradation of PUMA and BAX in a protein kinase AKT1-dependent manner to promote cancer cell proliferation and tumor growth. Interestingly, inactivation of AKT1 results in activation of another protein kinase GSK3α/β, which facilitates the proteasomal degradation of FBXL20 by another F-box protein, FBXO31. Thus, a switch between two signaling kinases AKT1 and GSK3α/β modulates the functional activity of these proapoptotic regulators, thereby determining cell survival or death. RNAi-mediated ablation of FBXL20 results in increased levels of PUMA as well as BAX, which further enhances the sensitivity of cancer cells to chemotherapeutic drugs. We showed that high level expression of FBXL20 in cancer cells reduces therapeutic drug-induced apoptosis and promotes chemoresistance. Overall, this study highlights the importance of targeting FBXL20 in cancers in conjunction with chemotherapy and may represent a promising anticancer strategy to overcome chemoresistance.

The phenomenon of programmed cell death (apoptosis) is a conserved cellular mechanism to maintain homeostasis during development and aging (1). Cells undergo apoptosis by two distinct pathways, namely intrinsic and extrinsic pathway.

BCL2 family proteins (BCL-2 homology domain containing proteins) play important roles in determining the cell fate by regulating the mitochondrial membrane potential in the intrinsic pathway of apoptosis. BCL-2 family proteins are classified into antiapoptotic and proapoptotic proteins. PUMA (p53 upregulated modulator of apoptosis) and BAX (BCL2-associated X protein) are most well-known apoptotic inducers. Under normal condition, apoptotic activity of BAX is impaired by inhibitory interactions with antiapoptotic BCL-2 proteins (2–4). Upon death stimuli, PUMA contributes to the induction of apoptosis by promoting the disruption of BAX-BCL2 interaction and thereby release BAX from BAX-BCL2 complex (5, 6). Released BAX is then oligomerized on the mitochondrial membrane to lower the membrane potential, resulting in the release of cytochrome c and induction of apoptosis (7–9).

The expression of PUMA and BAX is largely regulated at the transcriptional level by tumor suppressor p53 (10–12). Therefore, presence of p53 activity in tumor increases the potency of chemotherapeutic drugs through facilitating the induction of apoptosis. PUMA is also been shown to be regulated by other transcription factors such as p73, E2F1, and FOXO3a (13–16). Recent studies have demonstrated that both PUMA and BAX could be regulated at the proteasomal level in a phosphorylation-dependent manner (17–20), and this partly attributes to survival mechanisms of cancer cells (21). However, mechanistic basis of proteasomal regulation of PUMA and BAX by E3 ubiquitin ligases is largely unknown.

Human genome encodes for approximately 600 E3 ubiquitin ligases among which RING finger SCF (SKP1-Cullin1-F-box) E3 ubiquitin ligases are well studied and best known for targeting phosphorylated proteins for promoting their proteasomal degradation. SCF E3 ubiquitin ligases comprise of three invariable components (SKP1, Cullin1, and RBX1) and a variable component - F-box proteins. F-box proteins are associated with SKP1 through their conserved F-box motif to form SCF complex and function as substrate receptor (22, 23). Typically, F-box proteins recognize phosphorylated substrates and promote their polyubiquitination. Previous reports showed that phosphorylated form of PUMA and BAX is less

---

stable than nonphosphorylated form, indicating that SCF E3 ubiquitin ligase(s) might be involved in destabilization of PUMA and BAX (17–20).

In this study, we have identified FBXL20 as a potential regulator of proapoptotic proteins PUMA and BAX. We show that FBXL20 regulates PUMA and BAX at the post-translational level by promoting their degradation through 26S proteasome. FBXL20-mediated degradation of PUMA and BAX reduces the potency of chemotherapeutic drug-induced apoptosis and thereby promotes tumor growth. Our study revealed that inactivation of AKT1 results in the stabilization of BAX and PUMA due to the proteasomal degradation of FBXL20 by SCF^{FBXO31} E3 ubiquitin ligase in GSK3α/β-dependent manner. Thus, our study delineates an important cellular signaling pathway required to maintain the basal levels of proapoptotic regulators. Overall, we propose that targeting FBXL20 in cancers in conjunction with chemotherapy may be a promising anticancer strategy.

Results

FBXL20 functions as antiapoptotic protein by targeting PUMA and BAX

Proapoptotic genes, *PUMA* and *BAX*, are expressed at low levels in unstressed proliferating cells and rapidly induced in response to wide range of cellular stresses (5, 21). In general, induction of PUMA and BAX is considered to occur at the transcriptional level (7–16). However, recent studies indicated that stability of PUMA and BAX is also regulated at the posttranslational level (17, 18, 20). We therefore presumed that PUMA and BAX might be regulated at the proteasomal level and performed a screen wherein we ectopically expressed ORFs of 54 SCF-F-box proteins to identify putative F-box protein(s) that may regulate PUMA. From this screen, F box protein FBXL20 emerged as the potential candidate that reduced PUMA levels upon ectopic expression (Figs. 1*A* and S1*A*). Interestingly, we found that ectopically expressed FBXL20 also reduced BAX levels (Figs. 1*A* and S1*A*). To determine whether FBXL20 maintains physiological levels of PUMA and BAX, we generated FBXL20 stable knockdown (FBXL20-KD) MCF7 cells using two unrelated lentiviral shRNAs. As compared with the cells expressing nonsilencing shRNA (NS), the levels of PUMA and BAX were significantly increased in FBXL20-KD cells (Figs. 1*B* and S1*B*), while the levels of BIM and BCL2 were not affected by FBXL20 knockdown. However, the transcript levels of both *PUMA* and *BAX* were not altered in FBXL20-depleted cells (Fig. S1*C*).

An increase in PUMA and BAX levels upon FBXL20 knockdown in MCF7 cells indicated that FBXL20-depleted cells could be more sensitive to chemotherapeutic drugs than wild-type NS cells. We therefore performed a series of experiments to examine the sensitivity of FBXL20 knockdown cells to Doxorubicin (DOXO) and Camptothecin (CPT). First, we performed MTT assay in MCF7 cells expressing NS and FBXL20 shRNA with varying concentrations of either DOXO or CPT and evaluated 50% growth inhibitory concentration (IC50) of these drugs. As shown in Figure 1*C*, the IC50 values

of DOXO were ~2.7 fold less in FBXL20 knockdown cells (IC$_{50}$ 0.18 ± 0.05 μM) than that in NS cells (IC$_{50}$ 0.5 ± 0.09 μM). Consistent with this result, the IC50 values of CPT were also approximately threefold lower in FBXl20-KD cells (IC$_{50}$ 1.0 ± 0.25 μM) as compared with NS cells (IC$_{50}$ 3.0 ± 0.1 μM) (Fig. 1*C*). These results demonstrated that FBXL20 depletion increased the sensitivity to Doxorubicin or Camptothecin. We then performed clonogenic survival assay and results showed that FBXL20-KD cells showed an increased sensitivity to DOXO or CPT as compared with the NS cells treated with DMSO (Figs. 1, *D* and *E* and S1*D*). In contrast, knockdown of PUMA in FBXL20-KD cells resulted in formation of increased number of colonies as compared with FBXL20-KD cells treated with either DOXO or CPT indicating that increased levels of PUMA in FBXL20-KD increased sensitivity to chemotherapeutic agents, at least in part (Fig. 1, *D* and *E*). Next, we determined the apoptotic index of MCF7 cells expressing either NS shRNA or FBXL20 shRNA, or coexpressing FBXL20 and PUMA shRNAs or coexpressing FBXL20 shRNA and BAX shRNA following treatment of DOXO. FACS analysis of Annexin-V/7-AAD stained cells revealed that percentage of apoptotic cells was increased in FBXL20-KD cells as compared with NS cells, which further increased following treatment with DOXO or CPT (Figs. 1*F* and S1*E*). However, codepletion of PUMA or BAX in FBXL20 knockdown cells decreased the percentage of apoptotic cells as compared with the FBXL20-KD cells alone (Figs. 1*F* and S1*E*).

We next performed comet assay to determine whether increased level of apoptosis of DOXO/CPT treated FBXL20-KD cells was due to induction of DNA fragmentation. The results of comet assay demonstrated that FBXL20-KD cells were more susceptible to DNA fragmentation (as evident by the appearance of higher percentage of apoptotic comets and DNA in tail) as compared with the NS cells following treatment with either DOXO or CPT (Fig. 1, *G* and *H*). However, the extent of DNA tailing was significantly reduced upon knocked down of PUMA in FBXL20-KD cells, indicating that accumulated PUMA in FBXL20-KD cells could be responsible for induction of severe DNA damage (Fig. 1*H*). Conversely, ectopic expression of FBXL20 decreased DNA fragmentation and DNA tailing following treatment with either DOXO or CPT (Fig. S1, *F* and *G*). In addition to this, an ectopic expression of FBXL20 also inhibited the cleavage of caspase 9 and PARP1 induced by DOXO treatment, suggesting the role of FBXL20 in counteracting apoptosis (Fig. S1*H*).

Mitochondrial membrane potential alteration is one of the markers routinely measured to detect apoptotic cells. We then monitored the mitochondrial membrane potential using JC1 dye, which exhibits potential dependent fluorescence emission shift from red to green upon induction of intrinsic apoptosis. FACS analysis of cells expressing either vector or FBXL20, treated with CPT, and stained with JC1 dye showed that FBXL20 expressing cells display substantially less emission shift as compared with the cells expressing vector (Fig. 1*I*).

BAX oligomerization on mitochondrial outer membrane leads to membrane polarization, release of cytochrome c, and induction of apoptosis (9, 10). We found that FBXL20 also
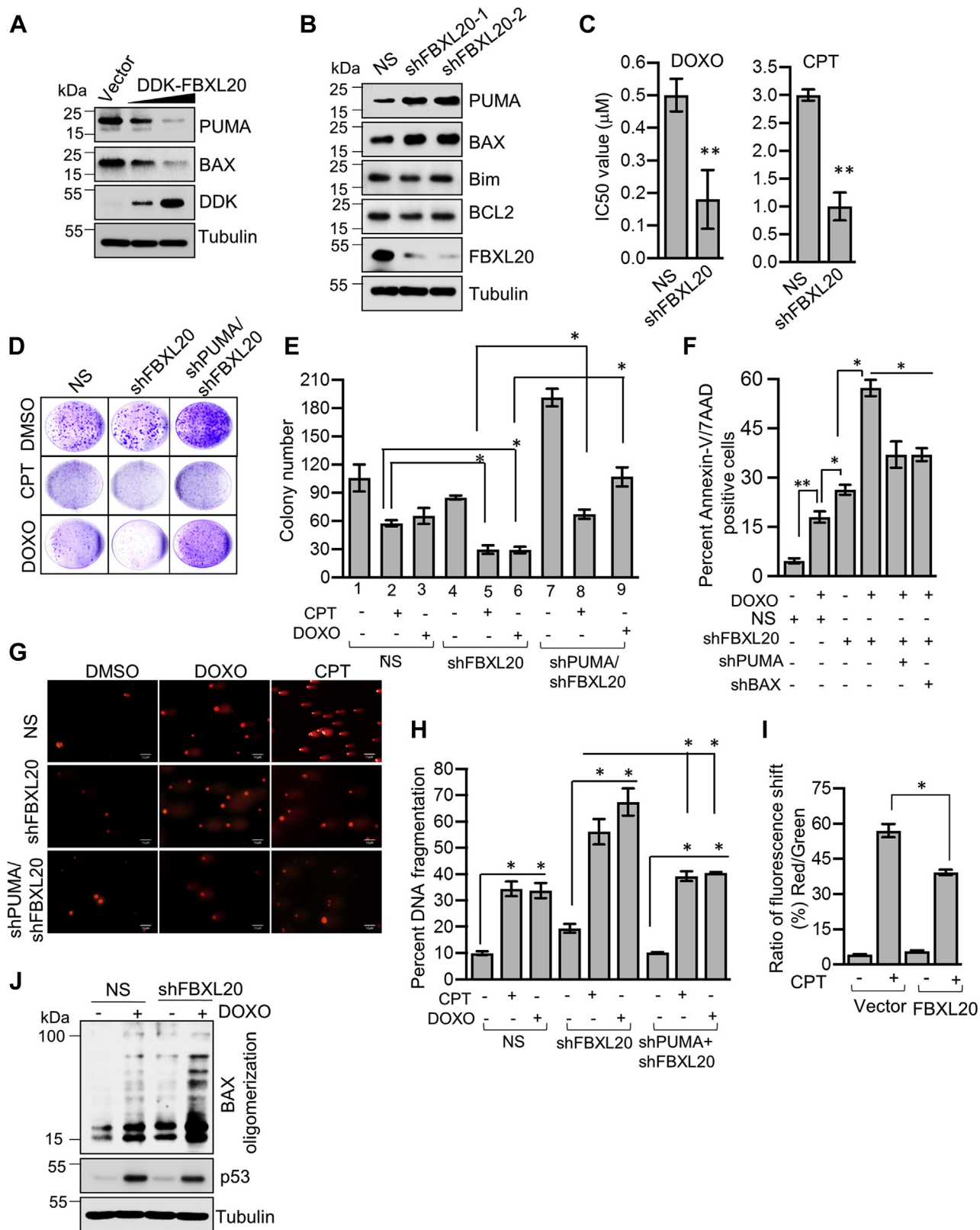
Figure 1. PUMA and BAX are the cellular target of FBXL20. *A*, immunoblot monitoring PUMA and BAX in MCF7 cells ectopically expressing either vector or DDK-FBXL20. *B*, immunoblot analysis in MCF7 cells expressing either nonsilencing shRNA (NS) or two unrelated FBXl20 shRNAs to detect PUMA, BAX, Bim, BCL2, and FBXL20. *C*, MTT assay monitoring 50% growth inhibitory concentration (IC50) of MCF-7 cells expressing either NS or FBXL20 shRNA treated with doxorubicin (DOXO) or camptothecin (CPT) for 24 h. Data are presented as the mean ± SD from three independent experiments. *D*, clonogenic assay monitoring survival of MCF-7 cells expressing either NS, FBXL20 or PUMA or PUMA and FBXL20 shRNAs treated with either 1 μM DOXO or 1 μM CPT for 24 h and allowed to grow for 15 days without drug and stained with 0.05% crystal violet. Experiment was repeated three times. *E*, quantitative analysis of clonogenic assay. Data are presented as the mean ± SD from three independent experiments. *F*, flow cytometry analysis of Annexin-V and 7AAD staining in MCF7 cells expressing either NS or FBXL20 shRNA or coexpressing PUMA and FBXL20 shRNAs or coexpressing BAX and FBXL20 shRNAs treated 5 μM

negatively regulates BAX (Fig. 1, *A* and *B*); we therefore, assessed the extent of BAX oligomerization in FBXL20-KD cells following treatment with Doxorubicin. Immunoblotting data showed that knockdown of FBXL20 resulted in an elevated level of BAX oligomers, which was further increased upon Doxorubicin treatment (Fig. 1*J*). DNA damaged-induced increased oligomerization of BAX in FBXL20-KD cells could be due to either the increased expression levels of BAX or the increased disruption of BAX-BCL2 interaction resulting from the increased levels of PUMA. To address these possibilities, we performed coimmunoprecipitation assay to examine BAX and BCL2 interaction in MCF7 cells expressing NS and FBXL20 shRNA treated with and without Doxorubicin. Immunoblotting results of immunoprecipitates showed that BAX and BCL2 interaction was disrupted in NS and FBXL20-KD cells treated with Doxorubicin (Fig. S1*I*). Therefore, increased oligomerization of BAX in FBXL20-KD cells could be due to both increase levels of BAX as well as disruption of BCL2-BAX interaction. Collectively, these results suggest that FBXL20 inhibits the induction of apoptosis by reducing the expression levels of proapoptotic proteins PUMA and BAX.

FBXL20 directs proteasomal degradation of PUMA and BAX through SCF complex

We next sought to understand the mechanism(s) by which FBXL20 regulates PUMA and BAX. To understand how FBXL20 reduces the levels of PUMA and BAX, we first examined mRNA level of PUMA and BAX upon ectopic expression of FBXL20. Real-time RT-PCR results showed that ectopic expression FBXL20 in MCF7 cells did not affect the mRNA levels of *PUMA* and *BAX* (Fig. 2, *A* and *B*). In contrast, protein levels of PUMA and BAX are significantly reduced by FBXL20 (Figs. 1*A* and S1, *A* and *B*). Generally, F-box proteins function by modulating activity of their substrates at the proteasomal level. We then examined whether PUMA and BAX are substrates of FBXL20 and are regulated at the proteasomal level. Consistent with this idea, treatment of cells with proteasomal inhibitor, MG132 inhibited the ability of FBXL20 to reduce expression levels of PUMA and BAX (Fig. 2*C*). This suggested that FBXL20-mediated reduction of PUMA and BAX protein level is a posttranscriptional event. Preceding results demonstrated that PUMA and BAX protein levels are increased upon FBXL20 knockdown (Fig. 1*B*). We therefore monitored PUMA and BAX protein turnover by cycloheximide chase assay. As shown in Figure 2, *D–F*, the turnover of PUMA and BAX decreased in FBXL20-KD cells (Fig. 2, *D–F*).

PUMA and BAX are known to be regulated at the transcriptional level predominantly by p53 (11, 12, 24). We

therefore sought to examine whether FBXL20-mediated degradation of PUMA or BAX was p53-dependent. Immunoblot data showed that ectopically expressed FBXL20 reduced the expression levels of BAX and PUMA in both p53-wild-type and p53-deficient cells, indicating that FBXL20-mediated degradation of PUMA and BAX was p53-independent (Fig. 2*G*)

Typically, F-box proteins associate with SCF complex through their F-box motif to promote substrate poly-ubiquitylation. To determine the involvement of F-box motif of FBXL20 in PUMA or BAX degradation, we generated F-box motif deletion mutant of FBXL20 (DDK-ΔF-FBXL20). Unlike wild type, ectopically expressed DDK-ΔF-FBXL20 failed to degrade both PUMA and BAX (Fig. 2, *H* and *I*), indicating that FBXL20 promotes the degradation of both PUMA and BAX *via* SCF complex.

FBXL20 interacts with PUMA and BAX and directs their degradation-specific K48-linked polyubiquitination

F-box protein-mediated degradation of their substrates requires an interaction with the substrates. To ascertain whether FBXL20 interacts with PUMA and BAX, we performed a series of coimmunoprecipitation experiments. First, we ectopically expressed DDK-tagged FBXL20 and HA-tagged PUMA in MCF7 cells and whole cell lysates were immunoprecipitated with anti-DDK or anti-HA antibodies, respectively. Figure 3*A* showed the presence of HA-PUMA in DDK-FBXL20 immunoprecipitates. The reciprocal immunoprecipitation showed the presence of DDK-FBXL20 in HA-PUMA immunoprecipitates (Fig. 3*A*). Consistent with this observation, the interaction of FBXL20 with PUMA and BAX was also observed at the endogenous level (Fig. 3*B*). In addition, we also examined physical interaction of PUMA and BAX with FBXL20 by an *in vitro* by GST pull-down assay. As shown in Figure 3, *C* and *D*, *in vitro* interaction between purified GST-PUMA or GST-BAX and His-FBXL20 was detected. These results confirm that FBXL20 directly interacts with BAX and PUMA. Given that BH3 domain in PUMA is involved in protein–protein interaction, we presumed that the FBXL20 might interact with BH3 domain of PUMA. To investigate this possibility, we ectopically expressed DDK-FBXL20 and HA-PUMA or HA-ΔBH3-PUMA in MCF7 cells and immunoprecipitated with either anti-DDK or anti-HA antibodies, respectively. As shown in Figure 3*E*, DDK-FBXL20 interacted with HA-PUMA and not with HA-ΔBH3-PUMA indicating that FBXL20 interacts with BH3 domain of PUMA. In agreement with previous study, we found that BH3 domain of PUMA is important to interact with BAX. Interestingly, immunoblotting of FBXL20 immunoprecipitates revealed that
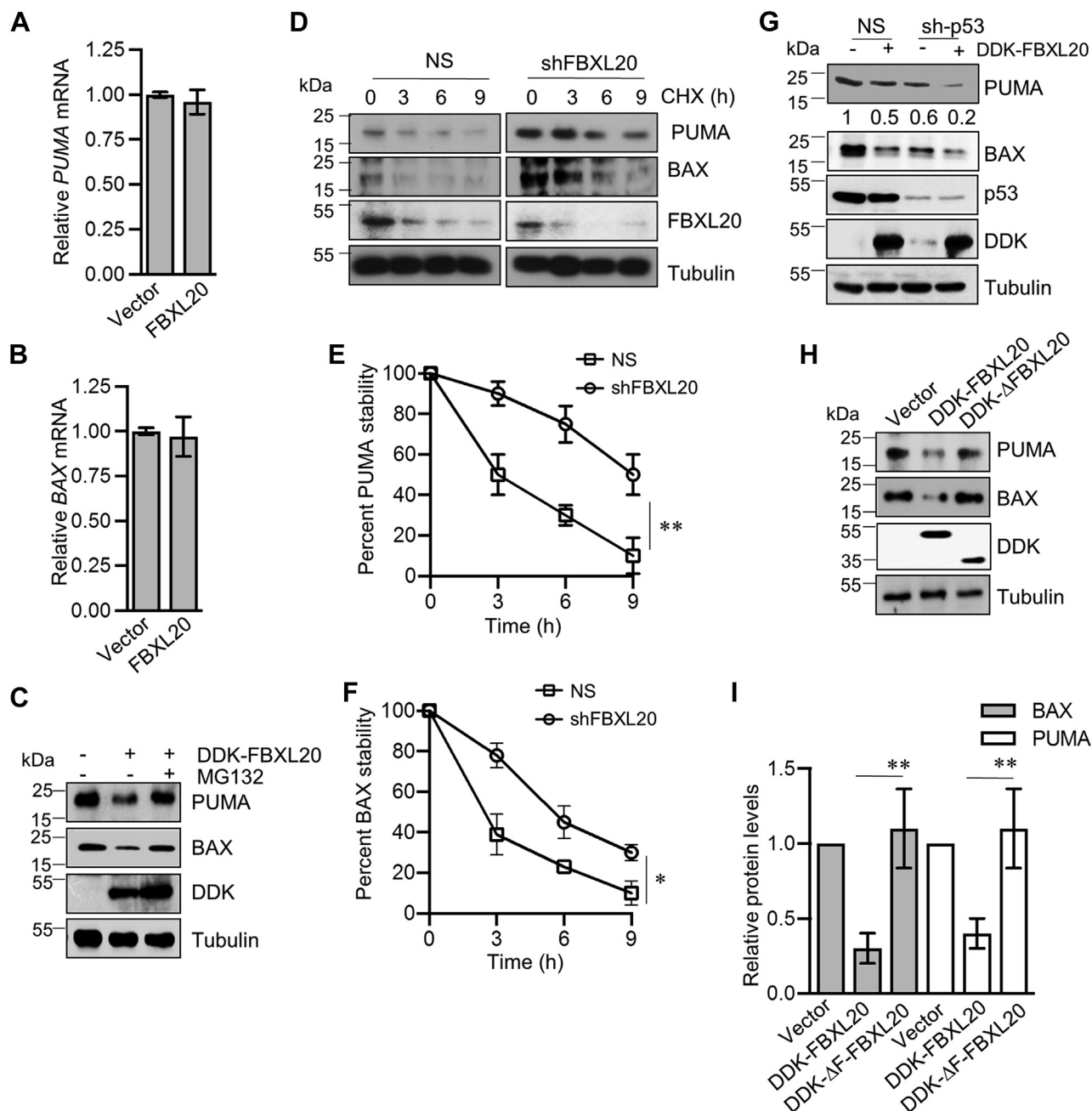
Figure 2. FBXL20 regulates PUMA and BAX at the proteasomal level through SCF complex. *A* and *B*, quantitative real-time RT-PCR monitoring the mRNA levels of *PUMA* and *BAX* expression in MCF7 cells expressing either vector or FBXL20. GAPDH was used as a normalizing control. Experiment was repeated three times. *C*, immunoblot monitoring the levels of PUMA and BAX in MCF7 cells transfected either vector or DDK-FBXL20. After, 42 h of transfection, cells were treated 5 µM MG132 for additional 6 h before harvesting. *D*, cycloheximide chase/immunoblot assay monitoring PUMA and BAX turnover in MCF7 cells expressing either NS or FBXL20 shRNA treated with cycloheximide (100 µg/ml) for the indicated time. The experiment was repeated three times. *E* and *F*, quantitative analysis of PUMA and BAX (panel *D*) using Image J. The graphs show the ratio of the relative levels of PUMA and tubulin (loading control) or BAX and Tubulin (loading control) at each time; The expression level was set to 100% at time "0". Data are presented as the mean ± SD from three independent experiments. *G*, immunoblot analysis monitoring PUMA and BAX levels in MCF7 cells stably expressing NS or p53 shRNA following ectopic expression of either vector or DDK-FBXL20. The experiment was repeated two times. *H*, immunoblot monitoring PUMA and BAX in MCF7 cells expressing either vector or DDK-FBXL20 or F-box deleted FBXL20 (DDK-ΔF-FBXL20). *I*, densitometric analysis of (*H*) using Image J quantifying relative proteins levels of PUMA and BAX. Data are presented as the mean ± SD from three independent experiments. For all immunoblot analysis tubulin was monitored as a loading control. **$p < 0.01$, *$p < 0.05$.

interaction of FBXL20 with BAX is independent of PUMA (Fig. 3*E*).

Typically, F-box proteins direct proteasomal degradation of their substrates by promoting their polyubiquitination (22, 25). We then asked whether FBXL20 promotes polyubiquitination

of PUMA and BAX. Ubiquitin possesses seven lysine residues (K6, K11, K27, K29, K33, K48, and K63) that may be utilized to form polyubiquitin chains. Among these lysine residues, K48-linked polyubiquitin chains are generally marked for proteasomal degradation of target proteins (26). We therefore
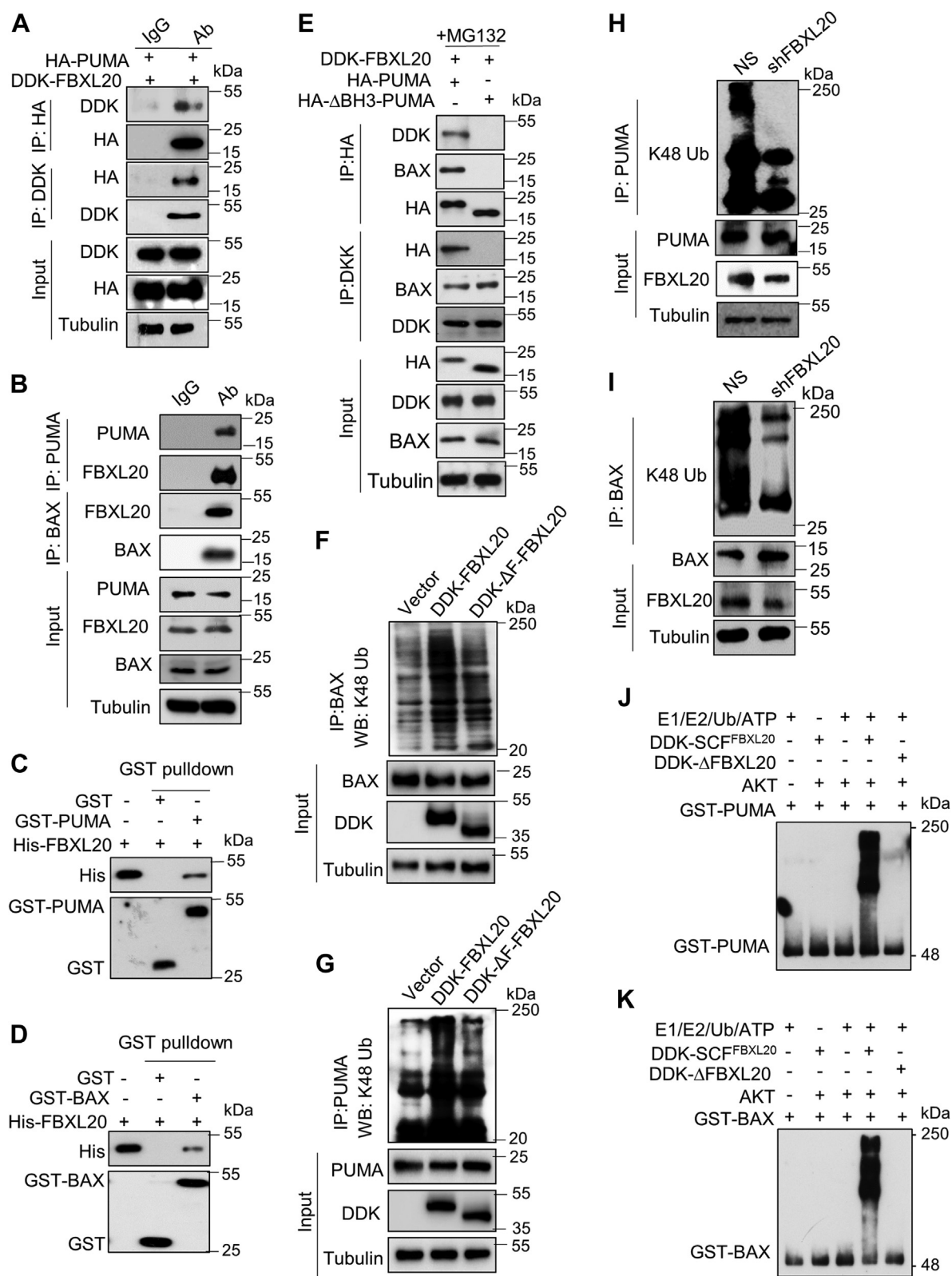
Figure 3. FBXL20 interacts with PUMA and BAX and directs their degradation-specific K48-linked polyubiquitination. *A*, co-immunoprecipitation assay monitoring the interaction between ectopically expressed PUMA and FBXL20. Whole cell lysates from MCF7 cells expressing HA-PUMA and DDK-FBXL20 were immunoprecipitated with either IgG or anti HA or anti DDK antibody as indicated. Cells were treated with MG132 (5 μM) was for 6 h prior to cell lysate preparation. *B*, coimmunoprecipitation assay monitoring endogenous interaction between PUMA and FBXL20 in MCF-7 cells. Whole cell lysates were immunoprecipitated with either IgG or anti-PUMA or anti-BAX antibody as indicated. Cells were treated with MG132 (5 μM) for 6 h prior to cell lysate preparation. *C* and *D, in vitro* GST pull-down assay. GST-agarose bead bound GST-PUMA or GST-BAX protein, or GST alone was incubated with purified His-FBXL20. After wash, the bead bound proteins were released by boiling with 1× Laemmli buffer. Eluted protein samples were immunoblotted with anti-His and GST antibodies. His-FBXL20 protein used as an input (5%). *E*, coimmunoprecipitation assay in MCF-7 cells ectopically expressing DDK-FBXL20 or HA-

examined whether FBXL20 promotes K48-linked poly-ubiquitination of BAX and PUMA. Immunoprecipitation of MCF7 cell extracts expressing either vector or DDK-FBXL20 or DDK-ΔF-FBXL20 with BAX and PUMA antibodies followed by immunoblotting with K48 linked Ub antibody showed that DDK-FBXL20 promoted K48-linked poly-ubiquitination of PUMA (Fig. 3F) and BAX (Fig. 3G). However, the knockdown of FBXL20 reduced K48-linked ubiquitination of PUMA (Fig. 3H) and BAX (Fig. 3I). Consistent with these results, *in vitro* ubiquitination assay also demonstrated that FBXL20 can promote the poly-ubiquitination of recombinant PUMA and BAX (Fig. 3, *J* and *K*). Collectively, these results suggested that FBXL20 interacts with PUMA and BAX and promotes polyubiquitination to direct their proteasomal degradation.

AKT1-mediated phosphorylation of BAX and PUMA is required for recognition and proteasomal degradation by FBXL20

Typically, proteins undergo posttranslational modification such as phosphorylation prior to their ubiquitination by E3 ubiquitin ligase (25, 26). Previous studies showed that phosphorylation of BAX at Ser184 by AKT and PUMA at Ser10 by IKK kinases regulates their activity and hence apoptosis (17, 18, 27). It was also proposed that inactivation of PI3K-AKT pathway results in stabilization of PUMA (28). In agreement with the previous studies, we also observed that total phospho-serine levels of PUMA and BAX were reduced following inhibition of AKT1 (Fig. S2A). Further, BAX and PUMA levels were increased following inactivation of AKT1 by using a chemical inhibitor (Figs. 4A and S2B). Consistent with these results, shRNA-mediated knockdown of AKT1 also results an increased level of BAX and PUMA (Figs. 4B and S2C). However, AKT1 inhibition did not affect the mRNA levels of *PUMA* and *BAX* (Fig. S2D).

We then asked whether FBXL20 is involved in AKT1-mediated destabilization of PUMA and BAX. To test this, we ectopically expressed either vector or FBXL20 in MCF7 cells in the presence or absence of an AKT inhibitor. Immunoblot results showed that degradation of PUMA and BAX by FBXL20 was significantly inhibited following inhibition of AKT1, indicating that FBXL20 might be targeting AKT-mediated phosphorylated form of PUMA and BAX (Figs. 4C and S2E). Further, we observed that AKT inhibition also resulted in significant loss of interaction of FBXL20 with PUMA and BAX (Figs. 4D and S2F). Consequently, FBXL20-mediated K48-linked polyubiquitination of PUMA and BAX was also markedly reduced upon AKT1 inactivation (Fig. 4, *E* and *F*).

Previous study showed that Ser10 phosphorylation of PUMA is important for its proteasomal stability (17, 18). We

therefore asked whether Ser10 phosphorylation in PUMA is important for FBXL20-mediated degradation. To address this, we coexpressed FBXL20 with either wild-type PUMA or phosphorylation defective mutant PUMA(S10A). Immunoblotting results showed that ectopically expressed FBXL20 degraded wild-type PUMA but failed to promote degradation of PUMA(S10A) mutant (Fig. 4G) indicating that phosphorylation of PUMA at Ser10 is important for its degradation.

Similar to PUMA, the serine 184 phosphorylation of BAX by AKT1 is critical for its activity. Consistent with above results, ectopically expressed FBXL20 failed to degrade phosphorylation defective BAX(S184A) mutant indicating that FBXL20 targets phosphorylated form of BAX (Fig. 4H). To further authenticate this observation, we examined the poly-ubiquitinated levels of wild-type and mutant PUMA(S10A). Results revealed that ectopically expressed FBXL20 also failed to promote K48-linked polyubiquitination of PUMA(S10A) mutant (Fig. 4I). Collectively, these results suggested that AKT-mediated phosphorylation of PUMA at Ser10 and BAX at Ser184 is indispensable for their recognition and proteasomal degradation by FBXL20.

AKT inactivation results in FBXO31-mediated proteasomal degradation of FBXL20

Our preceding results showed that AKT1-mediated phosphorylation of PUMA is essential for its recognition as well as polyubiquitination by FBXL20. We also observed that FBXL20 levels gradually decreased in a dose-dependent inhibition of AKT1, with no apparent change in FBXL20 mRNA level (Figs. 4A and S3A). We speculated that inactivation of AKT1 could stabilize some other factor(s) or E3 ubiquitin ligase, which in turn may target FBXL20 for degradation. To address this, we first examined whether FBXL20 is proteasomally regulated upon inactivation of AKT1. As shown in Figure 5A and Fig. S3B, levels of FBXL20 were decreased upon treatment with an AKT1 inhibitor; however, addition of proteasome inhibitor MG132 blocked FBXL20 ablation, indicating that AKT1 inactivation-mediated reduction of FBXL20 level occurs at the proteasomal level.

Our previous study demonstrated that inactivation of AKT1 either by pharmacological inhibitor or RNAi-mediated depletion leads to accumulation of tumor suppressor F-box protein FBXO31 (29). We therefore examined the possibility of whether FBXO31 could facilitate proteasomal degradation of FBXL20. Indeed, immunoblotting results showed that ectopically expressed FBXO31 markedly reduced the levels of FBXL20, which was blocked following addition of MG132 (Figs. 5B and S3C). This observation suggested that ectopically expressed FBXO31 promoted proteasomal degradation of FBXL20 (Fig. 5B). We next tested whether FBXO31 is involved

---

PUMA or HA-ΔBH3-PUMA. Whole cell lysates were immunoprecipitated with either anti HA or anti DKK antibodies as indicated. MG132 (5 μM) was added for 6 h prior to cell harvesting. *F* and *G*, K48-linked polyubiquitination of PUMA and BAX. Whole cell lysates from MCF7 cells expressing either vector or DDK-FBXL20 or DDK-ΔF-BXL20 were immunoprecipitated with anti-PUMA (panel *F*) anti-BAX antibody (panel *G*). Immunoprecipitates were immunoblotted with lysine-48 linkage specific ubiquitin (K48-Ub) antibody. *H* and *I*, whole cell lysates from MCF7 cells expressing NS or FBXL20 shRNA were immunoprecipitated with anti-PUMA (panel *H*) or anti-BAX (panel *I*) antibodies. Immunoprecipitates were immunoblotted with lysine-48 linkage-specific ubiquitin (K48 Ub) antibody. *J* and *K*, *in vitro* ubiquitination assay monitoring the ability of SCF-FBXL20 and DDK-ΔF-BXL20 to polyubiquitinate PUMA (panel *J*) and BAX (panel *K*). For all immunoblot analysis tubulin was monitored as a loading control. IP, immunoprecipitation.
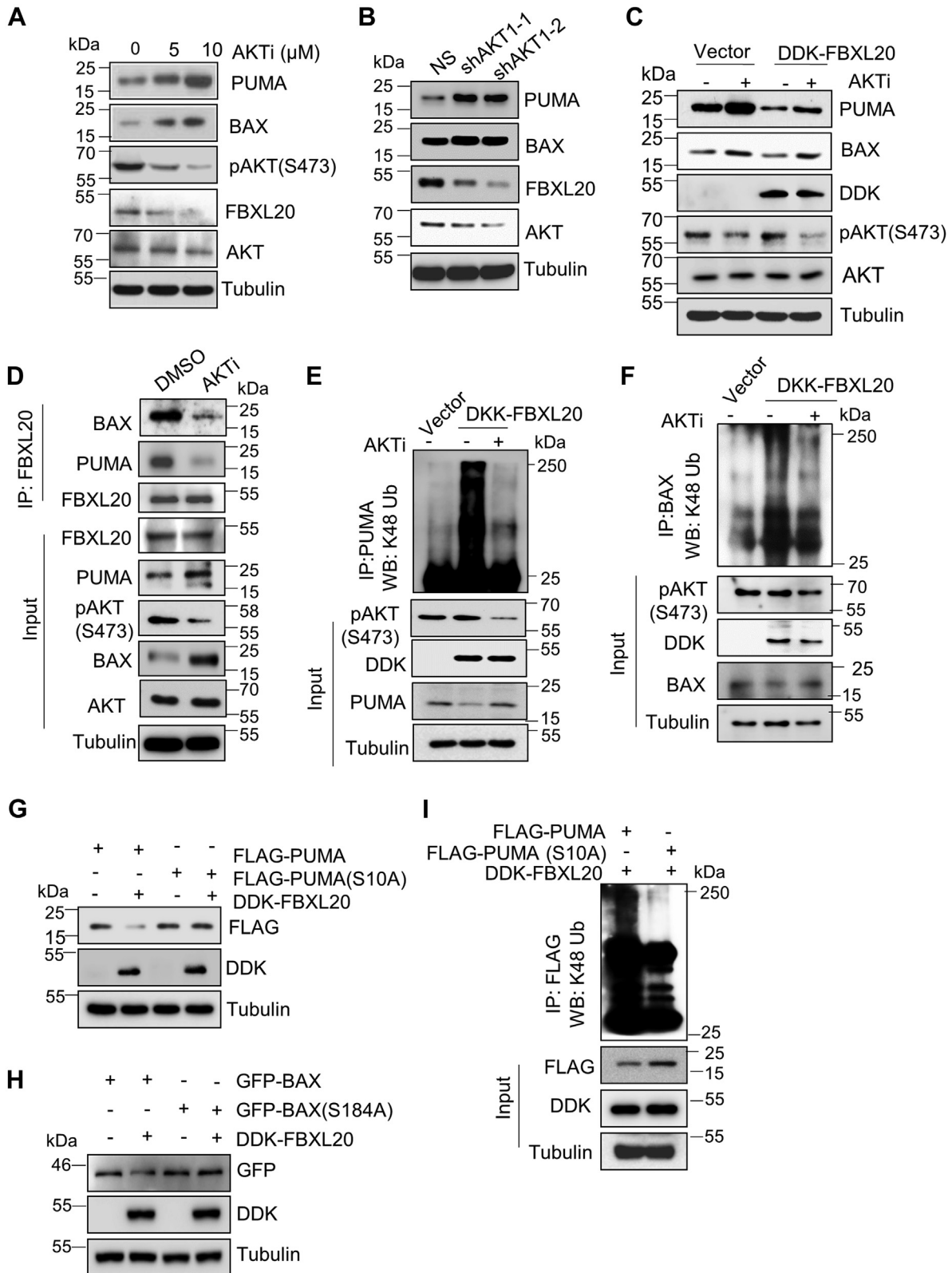
Figure 4. AKT-mediated phosphorylation of BAX and PUMA facilitates proteasomal degradation by FBXL20. *A*, immunoblot monitoring expression levels of PUMA, BAX, pAKT(S473), AKT, and FBXL20 in MCF7 cells treated with indicated concentrations of AKT inhibitor for 12 h. Experiment was repeated three times. *B*, immunoblot monitoring the expression levels of PUMA, BAX, FBXL20, and AKT in MCF7 cells expressing either NS or two unrelated AKT shRNAs (shAKT-1, shAKT-2). Experiment was repeated two times. *C*, immunoblot monitoring PUMA and BAX in MCF7 cells transfected with either vector or DDK-FBXl20. At 36 h post transfection, cells were treated with AKT inhibitor (5 μM) for additional 12 h. Experiment was repeated two times. *D*, coimmunoprecipitation monitoring endogenous interaction of FBXL20 with PUMA and BAX in the presence or absence of AKT inhibitor. *E* and *F*, K48-linked ubiquitination of PUMA in MCF7 cells expressing either vector or DDK-FBXL20 treated with AKT inhibitor(5 μM) for 12 h. Whole cell lysates were immunoprecipitated with either anti-PUMA (panel *E*) or anti-BAX antibody (panel *F*). Immunoprecipitates and input protein extracts were immunoblotted with

in proteasomal degradation of FBXL20 following AKT inactivation. The shRNA-mediated stable knockdown of FBXO31 in MCF7 cells resulted in an increased level of FBXL20 (Figs. 5C and S3D). Interestingly, AKT1 inactivation-mediated proteasomal degradation of FBXL20 was inhibited in FBXO31 knockdown cells (Figs. 5C and S3D). Further, cycloheximide chase/immunoblot assay revealed that the half-life of FBXL20 significantly increased in FBXO31-depleted cells (Figs. 5D and S3E). Finally, we examined the polyubiquitinated levels of FBXL20 following overexpression or depletion of FBXO31. Immunoblotting results of immunoprecipitates showed that ectopically expressed FBXO31 promoted K48-linked polyubiquitination of FBXL20 (Fig. 5E). In contrast, K48-linked polyubiquitination of FBXL20 was reduced in FBXO31-depleted cells (Fig. 5F). Collectively, these results suggested that FBXO31 regulates physiological levels of FBXL20.

We then investigated how AKT1 inactivation facilitates proteasomal degradation of FBXL20 by FBXO31. We observed that interaction of FBXO31 and FBXL20 was increased following AKT1 inactivation (Fig. 5G), indicating that AKT may play an important role in maintaining the cellular levels of FBXL20 through inhibiting the interaction of FBXO31 and FBXL20.

Previous study showed that AKT1 inactivation leads to the activation of GSK3α/β, which plays an important role in apoptosis (27). We then speculated that GSK3α/β might be involved in degradation of FBXL20 mediated by FBXO31. Immunoblotting data showed that FBXO31-mediated reduction of FBXL20 levels was significantly blocked following inactivation of GSKα/β using chemical inhibitors, BIO and LiCl (Fig. 5H). To understand the incompetency of FBXO31 to facilitate degradation of FBXL20 following inactivation of GSKα/β, we examined the interaction between FBXO31 and FBXL20 in the absence and presence of GSK3α/β signaling. Immunoblotting of immunoprecipitates revealed that interaction of FBXO31 and FBXL20 was reduced following inactivation of GSK3α/β (Fig. 5I). This suggests that GSK3α/β might phosphorylate FBXL20, which is required for interaction of FBXO31 and FBXL20.

We then searched for consensus phosphorylation motifs (S/TXXXS/T) of GSK3α/β in FBXL20 protein and *in silico* analysis predicted the presence of four consensus motifs (Fig. S3F). Hence, we explored the possibility of GSK3α/β involvement in phosphorylation and degradation of FBXL20 by FBXO31. We tested whether the interaction between FBXO31 and FBXL20 was dependent on phosphorylation by GSK3α/β. To address this, we analyzed total pSer levels in FBXL20 immunoprecipitates following treatment with either AKT1 or GSK3α/β inhibitor. Results revealed an increase in pSer levels of FBXL20 following AKT inactivation (Fig. 5J). However, GSK3α/β inhibition resulted in reduced pSer level in

FBXL20 immunoprecipitates indicating that GSK3α/β phosphorylated FBXL20 (Fig. 5J). To identify the GSK3α/β phosphorylation sites in FBXL20, four His-FBXL20 truncated constructs were generated and purified (Fig. S3, G–I). We then performed *in vitro* kinase assay using bacterially purified FBXL20 truncated proteins following incubation with GSK3α/β in the absence and presence of ATP. Immunoblotting of reaction mixtures with phospho-Serine or phospho-Threonine antibody revealed that three phosphorylation consensus motifs present in FBXL20 located at S139/S143, S251/S255, and T417/S421/S425 were phosphorylated by GSK3α/β (Fig. 5K). Collectively, these results suggest that activation of GSK3α/β signaling predisposes proteasomal degradation of FBXL20 by FBXO31.

High-level expression of FBXL20 is closely associated with breast cancer pathogenesis

Preceding results showed that FBXL20 impairs the apoptotic function of PUMA and BAX by promoting their proteasomal degradation (Figs. 1–3). We therefore reasoned that FBXL20 might be highly expressed in cancer and monitored FBXL20 protein levels in a panel of breast cancer cell lines. Immunoblotting results revealed that FBXL20 levels were substantially higher in metastatic breast cancer lines MDA-MB-231 and MDA-MB-435 cells as compared with MCF7 (breast adenocarcinoma) (Fig. 6A). Immunoblotting result also showed that the PUMA and BAX levels were significantly reduced in MDA-MB-231 and MDA-MB-435 cells compared with MCF7 cells (Fig. 6A). To validate cell line data, we examined the expression levels of BAX, PUMA, FBXL20, and FBXO31 in a panel of matched normal breast tissue and different grades of breast cancer specimens by immunohistochemistry (IHC). Analysis of IHC data demonstrated that FBXL20 levels were significantly increased in higher grades of breast cancer as compared with normal breast tissue (Fig. 6, B and C). We also observed an inverse correlation in expression of PUMA/BAX and FBXL20 in breast cancer patient samples (Fig. 6, B and C). Interestingly, expression levels of FBXL20 and FBXO31 are also conversely correlated (Fig. 6, B and C). We then asked whether FBXL20 has role in tumor growth through monitoring PUMA expression. Toward this, MDA-MB-231 cells stably expressing either nonsilencing (NS) shRNA or FBXL20 shRNA or FBXL20 and PUMA shRNA were subcutaneously implanted into NOD-SCID mice and tumor growth was monitored for the indicated time periods. Xenograft result showed that tumor growth of FBXL20 knockdown cells is slower as compared with NS expressing cells (Fig. 6D). However, co-knockdown of PUMA in FBXL20 knockdown cells results in tumor growth that is lesser that the NS cells but higher than the FBXL20

---

indicated antibodies. *G*, MCF7 cells were coexpressing DDK-FBBXL20 and FLAG-PUMA or FLAG-PUMA(S10A) as indicated for 48 h. Whole cell protein extracts were immunoblotted for the indicated proteins. Experiment was repeated two times. *H*, MCF7 cells were coexpressing DDK-FBBXL20 and GFP-BAX or GFP-BAX (S184A) as indicated for 48 h. Whole cell protein extracts were immunoblotted for the indicated proteins. Experiment was repeated two times. *I*, K48-linked ubiquitin of PUMA in MCF7 cells coexpressing DKK-FBXL20 and FLAG-PUMA or FLAG-PUMA(S10). Whole cell lysates were immunoprecipitated with anti-FLAG and immunoprecipitates were immunoblotted with K48-Ub antibody. Experiment was repeated two times. For all immunoblot analysis tubulin was monitored as a loading control. IP, immunoprecipitation.
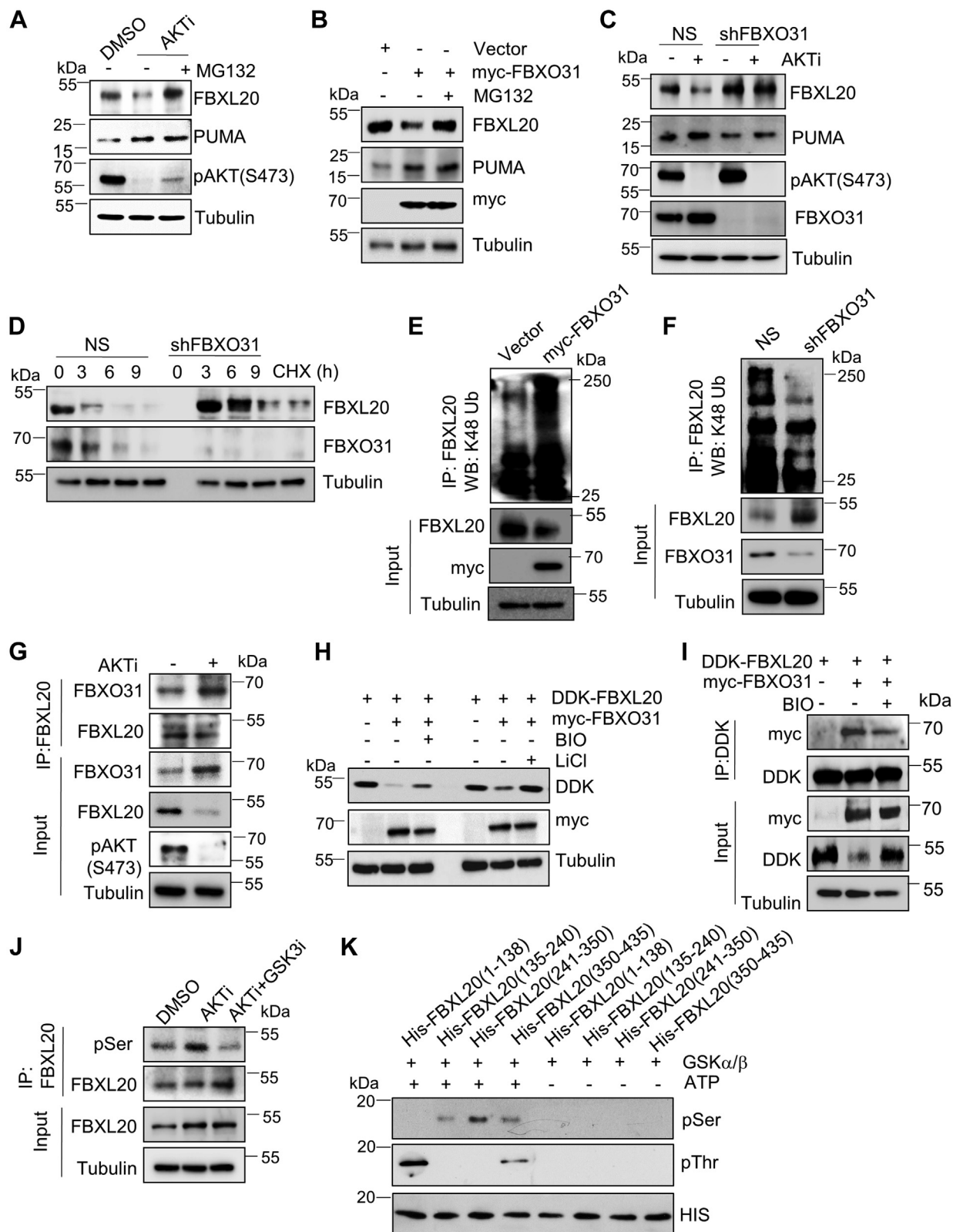
Figure 5. AKT inhibition leads to proteasomal degradation of FBXL20 by FBXO31. *A*, immunoblot monitoring FBXL20, PUMA and pAKT(S473) levels in MCF7 cells treated with AKT inhibitor for 12 h in the absence or presence of 5 μM MG132 as indicated. Cells were treated with MG132 for 6 h before harvesting. Experiment was repeated three times. *B*, immunoblot monitoring FBXL20 and PUMA level in MCF7 cells transfected with either vector or myc-FBXO31. At 42 h post transfection, cells were treated with 5 μM MG132 for additional 6 h prior to lysate preparation as indicated. Experiment was repeated three times. *C*, immunoblot monitoring the expression levels of FBXL20, PUMA, BAX, and phospho-AKT(Ser473) in MCF7 cells expressing either nonsilencing shRNA (NS) or FBXO31-shRNA (shFBXO31). Cells were treated with AKT inhibitor for 12 h as indicated. Experiment was repeated two times. *D*, cycloheximide chase/immunoblot assay monitoring FBXL20 turnover in MCF7 cells expressing NS or FBXO31 shRNA treated 100 μg/ml cycloheximide for the indicated time periods. Experiment was repeated three times. *E*, K48-linked ubiquitination of FBXL20 in MCF7 cells expressing either vector or myc-FBXO31. Whole cell

knockdown cells, indicating that FBXL20 plays crucial role in promoting tumor growth of MDA-MB-231 cells through reducing the PUMA level, at least in part (Fig. 6D). In addition, TCGA data analysis revealed that higher FBXL20 expression is closely associated with poor survival of breast cancer patients (Fig. 6E). These results demonstrated that FBXL20 could be a major driver of breast cancer malignancy and increased level expression of FBXL20 in higher grades of breast cancer could be partly due to reduced expression of FBXO31.

Collectively, these results demonstrated that lower levels of FBXO31 may lead to higher accumulation of FBXL20 in invasive breast cancers and subsequently reduce protein levels of PUMA/BAX, and that reduces sensitivity to conventional chemotherapeutic agents to induce cancer cell death. Hence, targeting FBXL20 or restoring FBXO31 may represent a potent anticancer mechanism in breast cancer.

Discussion

PUMA and BAX are among the most well-known proapoptotic members of BCL-2 family proteins. A large body of evidences suggests that PUMA and BAX are transcriptionally regulated by many transcription factors including p53 in response to diverse genotoxic stresses (11–16). In addition to transcriptional regulation, recent studies have highlighted that expression levels of PUMA and BAX could also be regulated at the proteasomal level in phosphorylation-dependent manner, suggesting the possible involvement of RING finger E3 ubiquitin ligases (17, 18, 27, 28, 30, 31). However, discovery of E3 ubiquitin ligase involved in proteasomal degradation of BAX and PUMA remained elusive. In this study, for the first time, we demonstrate the molecular mechanism of regulation of these proapoptotic proteins at the proteasomal level by SCF E3 ubiquitin ligase. We identified SCF^{FBXL20} E3 ubiquitin ligase that targets PUMA and BAX to promote their proteasomal degradation in AKT1 kinase pathway-dependent manner and thereby restricts their cellular level expression under normal condition as well as following drug treatment. Thus, this study demonstrated the fine-tuning regulation of proapoptotic regulators PUMA and BAX by FBXL20 at the posttranslational level to control the cell survival and apoptosis as summarized in model (Fig. 6F).

FBXL20 functions as an oncogene, and previous studies have shown that it promotes carcinogenesis through activation of β-catenin and c-Myc (32, 33). In agreement with previous studies, we also found that FBXL20 functions as an oncogene in breast cancer. The present study showed that FBXL20 is highly expressed in aggressive breast cancers to suppress the PUMA/BAX-mediated induction of apoptosis. Therefore, depletion of FBXL20 in breast cancer cells results in inhibition of cell proliferation and tumor growth. In addition, accumulation of PUMA and BAX in FBXL20-depleted cells predisposes them to vulnerable for apoptotic cell death by chemotherapeutic agents. Increased sensitivity of FBXL20-depleted cells to chemotherapeutic drugs indicates that targeting FBXL20 might help to overcome the chemotherapeutic resistance of cancer.

We show that FBXL20 contributes to suppress the induction of apoptosis by targeting BAX and PUMA for proteasomal degradation in the presence of persistent AKT1 signaling. AKT1 is constitutively activated in 70% breast cancer and plays an important role in cancer progression and malignancy. AKT is implicated as antiapoptotic regulator in many instances including irradiation and chemotherapeutic drugs treatment (28, 31). Therefore, inactivation of AKT1 results in induction of apoptosis and inhibition of tumor growth. However, it has been a long-standing question how inactivation of AKT1 leads to apoptosis (34, 35). Our study delineates an intricate molecular mechanism of apoptosis induction following inactivation of AKT1. We show that AKT plays a crucial role to inhibit apoptosis *via* two parallel pathways. It helps ablation of PUMA and BAX at the proteasomal level through accumulation of FBXL20. On the one hand, AKT1 phosphorylates PUMA (at serine 10) and BAX (at serine 184) to direct their proteasomal degradation by FBXL20. On the other hand, AKT1 suppresses the proteasomal degradation of FBXL20 by FBXO31.

Earlier it was reported that inactivation of AKT1 leads to activation of GSK3β, which in turn promotes apoptosis by phosphorylating BAX; however, molecular mechanism was obscure (36–38). In our previous study, we showed that AKT1 facilitates proteasomal degradation of FBXO31 through APC/C complex and therefore FBXO31 levels profoundly increase upon AKT1 inhibition (29). Here, we showed that phosphorylation of FBXL20 at multiple sites by GSK3α/β (upon AKT1 inactivation) serves as signal for degradation of FBXL20 by accumulated FBXO31 and thereby augments the cellular levels of PUMA and BAX. Of note, BCL2 interacts with BAX to prevent its apoptotic activity under normal proliferating condition. Upon accumulation, PUMA binds to antiapoptotic protein BCL2 and thereby releases BAX. BAX is then oligomerizes on the mitochondrial membrane to release cytochrome C leading to the activation of intrinsic pathway of apoptosis. Thus, AKT signaling plays an important role in escalating malignancy by impairing the cell death pathway through inactivation of GSK3 α/β–FBXO31–PUMA–BAX axis.

---

lysates were immunoprecipitated with anti-FBXL20 antibody and immunoblotted with K48-Ub antibody. F, K48-linked ubiquitination of FBXL20 in MCF7 cells expressing either NS or FBXO31 shRNA. Whole cell lysates were immunoprecipitated with anti-FBXL20 antibody and immunoblotted with K48-Ub antibody. G, coimmunoprecipitation monitoring endogenous interaction between FBXO31 and FBXl20 in MCF7 cells treated with or without AKT inhibitor (5 μM) for 12 h. H, MCF7 cells were cotransfected with plasmid expressing DKK-FBXL20, myc-FBXO31 as indicated for 36 h. Transfected cells were then treated with GSK3β inhibitor (1 μM BIO/2 mM LiCl) for 12 h as mentioned. Whole cell protein extracts were immunoblotted for the indicated proteins. I, coimmunoprecipitation assay monitoring the interaction of ectopically expressed DKK-FBXL20 with myc-FBXO31 in MCF7 cells treated with GSK3β inhibitor (1 μM BIO, 12 h). Whole cell protein extracts were immunoprecipitated with DDK antibody. Immunoprecipitates and input protein extracts were immunoblotted for the indicated proteins. J, MCF7 cells were treated with either DMSO (control) or inhibitors as indicated for 12 h. WCL were immunoprecipitated with anti-FBXL20 antibody. Immunoprecipitates and input protein extracts were immunoblotted for the indicated proteins. K, in vitro kinase assay was performed to examine the phosphorylation of FBXL20 by GSK3α/β. Bacterially purified different fragments of FBXL20 as indicated were incubated with immunopurified GSK3α/β kinase in presence and absence of ATP, and the reactions mixture were immunoblotted with anti-phospho-serine (pSer) and anti-phospho-threonine (pThr) antibodies. For all immunoblot analysis tubulin was monitored as a loading control. IP, immunoprecipitation.
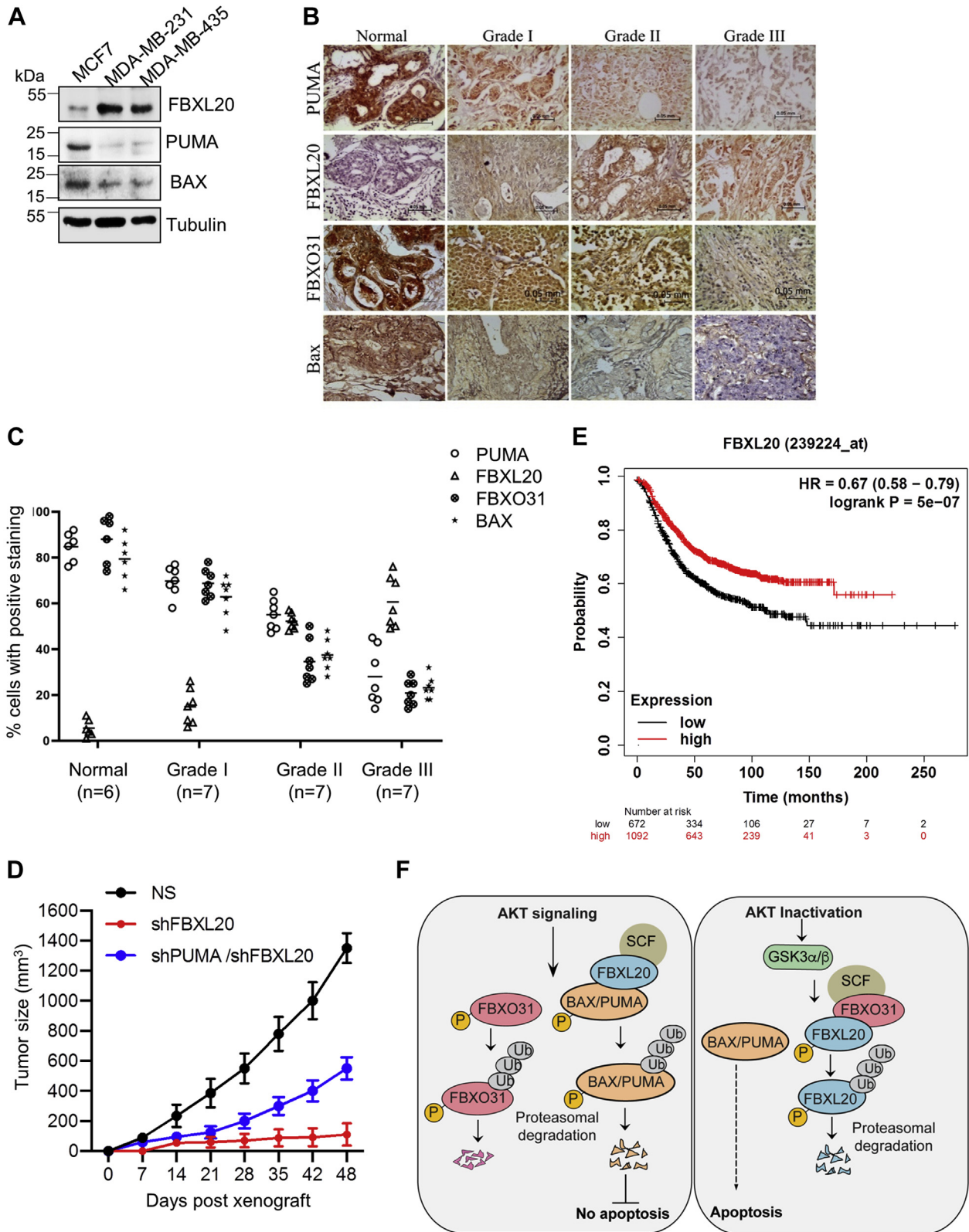
Figure 6. FBXL20 and FBXO31 are conversely correlated in breast cancer. *A*, whole cell lysates were immunoblotted for the indicated proteins. *B*, immunohistochemistry (IHC) monitoring FBXL20, FBXO31, PUMA, and BAX in normal breast (n = 6) and different grades of breast cancer specimens (n = 7). *C*, quantification of IHC. Staining intensity of PUM, BAX, FBXL20, and FBXO31 tissue was graded on a scale of 0 (no staining) to 3+ (strong staining). The protein expression was scored based on the percentage of positive cells. Data are presented as the mean ± SD. *D, in vivo* tumor growth. NOD-SCID mice were xenografted with MDA-MB-231 cells expressing either NS or FBXL20-shRNA or FBXL20 and PUMA shRNAs. Data are presented as the mean ± SD from one independent experiment with four mice (n = 4) per group. *E*, higher FBXL20 expression is closely associated with poor survival of breast cancer patients. *F*, model showing regulation of PUMA and BAX by FBXL20.

In conclusion, we discover the involvement of SCF complex in posttranslational regulation of proapoptotic proteins BAX and PUMA and deciphered the intriguing molecular mechanism that addresses the long-standing question of cell death following AKT1 inhibition. Most anticancer drugs exploit the apoptotic signaling pathways to trigger cancer cell death. Defects in the cell death pathways may result in drug resistance to limit the efficacy of anticancer therapy. Thus, a better understanding of the regulators apoptotic cell death signaling pathways may improve the efficacy of cancer therapy and overcome the chemotherapeutic drug resistance. Hence, the ability of cancer cells to induce PUMA or BAX in response to a treatment regimen might represent potential antitumor therapy. Therefore, our study suggests that targeting FBXL20 in breast cancers might help to overcome the chemoresistance and thus represent a promising anticancer strategy in conjunction with chemotherapy.

Experimental procedures

Cell lines, cell culture, and drug treatments

Human breast cancer cell lines MCF7, MDA-MB-231, MDA-MB-435 and human embryonic kidney cell HEK-293T were kindly provided by Prof. Michael R. Green (University of Massachusetts Medical School, USA). HEK-293T and MCF7 cells were cultured in high-glucose Dulbecco's modified Eagle's medium (DMEM) medium, MDA-MB-231, MDA-MB-435 cells were cultured in RPMI media containing 10% FBS at 37 °C incubator with 5% CO_2. Cells were treated with 5 μM AKT inhibitor (Calbiochem, 124005), 1 μM BIO (Cayman, 667463-62-9), and 2 μM LiCl for 12 h. In total, 5 μM MG132 (Calbiochem, 474790) was added as indicated. Doxorubicin (Sigma, D4035) and Camptothecin (Sigma, C9911) treatment was given as indicated in respective figure legends.

Plasmids, cloning, and mutagenesis

pCMV-myc-FBXO31 plasmid was kindly provided by Prof. David F. Callen (University of Adelaide, Australia). DDK-FBXL20 was purchased from Origene. His-Ub, HA-PUMA, HA-ΔBH3-PUMA, HA-BAX, EGFP-BAX, and EGFP-BAX (S184A) were purchased from Addgene. GST-PUMA plasmid was kindly provided by Dr Nam-Chul Ha (Seoul National University, Republic of Korea). PUMA cDNA was cloned in p3XFLAG-CMV-14 vector (Sigma) at BamHI site. FLAG-PUMA (S10A) mutant was generated by site-directed mutagenesis. F-box motif deleted FBXL20 mutant (DDK-ΔF-FBXL20) was generated by using FBXL20 as a template, and PCR product was inserted into SgfI and MluI site of the pCMV6-entry vector. FBXL20 truncations (1–138, 135–240, 241–350, and 350–436 aa) were PCR amplified and cloned into pET21a vector (EMD Biosciences). List of all primer sequences used in cloning is given in Table S1

Transfection and RNAi-mediated stable knockdown

Transfections were performed using polyethyleneimine-PEI-25K (Polysciences, #23966-1). Cells were seeded 1 day prior to transfection, and next day, transfection mixture was prepared in 150 mM NaCl solution by mixing DNA and polyethylenimine in the ratio of 1:2.4. Transfection mixtures were incubated at room temperature for 15 min and then added to the cells. Next day, media was changed and transfected cells were collected at the indicated time periods.

All lentiviral shRNA clones were kindly provided by Prof. Michael R. Green (University of Massachusetts Medical School, USA). Stable knockdown cells were generated as described previously (29). Briefly, HEK-293T cells were transfected with lentivirus shRNA plasmid along with packaging plasmids (pPAX2 and pMD2.G) using polyethyleneimine in a ratio of 1:1:0.5. Virus supernatants were collected at 48 h posttransfection and filtered through 0.45 μm syringe filter. For generating knockdown cell lines, cells were stably transduced in the presence of polybrene (8 μg/ml) with the shRNA lentiviruses. Transduced cells were then selected with puromycin (2 μg/ml) for 5 to 7 days. Scrambled nonsilencing shRNA (NS) was used as a control. shRNA sequences are listed in Table S2.

Immunoblotting analysis and coimmunoprecipitation

For immunoblot analysis, cells were harvested and washed with ice-cold PBS and lysed in lysis buffer (50 mM Tris PH 7.4, 5 mM EDTA, 250 mM NaCl, 50 mM NaF, 0.5 mM sodium orthovanadate, and 0.5% Triton X-100) containing protease inhibitor cocktail (Pierce, #88266) to prepare whole cell extracts. Protein concentrations were measured by Bradford method (39). The proteins were resolved in SDS–polyacrylamide gel electrophoresis, transferred to polyvinylidenedifluoride (PVDF) membrane, and detected by the specific antibodies. For coimmunoprecipitation assays, MCF7 cells were cotransfected with indicated plasmids for 40 h and then treated with 5 μM MG132 for 8 h. Transfected cells were then collected, washed with cold PBS, and protein extracts were prepared as described above. For endogenous interaction, cells were treated with 5 μM MG132 for 8 h as indicated, and then protein extracts were prepared as described above. Protein extracts (800 μg) were incubated with 2 μg of respective antibodies overnight at 4 °C with gentle rocking, followed by incubation with rProtein G agarose beads (Invitrogen, #15920-010) for 2 h at 4 °C. Beads were washed with lysis buffer three times, and the immunoprecipitates were eluted by boiling the beads in 1× laemmli buffer for 5 min. Eluted immunocomplexes were resolved on SDS-PAGE and immunoblotted with respective antibodies. Signal was detected using an appropriate HRP-conjugated secondary antibody and ECL reagents (Pierce).

Antibodies

Following antibodies were used: anti-FBXO31 (F4431), anti-FLAG (F1840), anti-phosphoserine (P5747), anti-phosphothreonine (P6623) and anti-tubulin (T5168) from Sigma. Anti-FBXL20 (TA306520) and anti-DDK (TA50011) from Origene. Anti-myc (#11667149001) from Roche. Anti-His (sc-8036), anti-cleaved PARP-1(sc-56196), anti-HA (sc-7392), anti-BIM (sc-374358), anti-GFP (sc-9996),

anti-p53 (sc-126) anti-GSKa/b (sc-7291) from Santacruz. Anti-PUMA (#4976), BAX (#2772), anti-AKT1 (#9272), anti-pAKT473 (#4058), anti-cleaved Caspase-9 (#9501), anti-K48-ubiquitin (#8081), anti-GST(#2624), anti-BCL2 (#4223) from Cell Signaling technology.

SCF-F-box screen

The ORFs of 54 F-box proteins cloned in the pCMV-myc expression vector were overexpressed individually in HEK-293T cells. The cells were collected after 48 h of transfection lysed in lysis buffer to prepare whole cell protein extracts. Protein samples were prepared, and the proteins were resolved by SDS-PAGE, transferred onto PVDF membrane, and probed with anti-PUMA antibody. This screen was repeated three times. The F-box protein showing maximum degradation for PUMA was then overexpressed in MCF7 cells to assess its activity on PUMA levels.

Cycloheximide chase

For the experiments monitoring stability of PUMA and BAX, MCF-7 cells expressing NS and FBXL20 shRNA were treated with cycloheximide (100 μg/ml) for 0, 3, 6, 9 h. Total cell extracts were subjected to immunoblotting with anti-PUMA, anti-BAX, and anti-tubulin antibodies. For experiment monitoring stability of FBXL20, MCF-7 cells expressing NS and FBXO31 shRNA were treated with cycloheximide as described above. Total cell extracts were subjected to immunoblotting with antiFBXL20 and anti-tubulin antibodies. Band intensities were quantified using Image J, and the ratio of the relative levels of PUMA or BAX or FBXl20 and tubulin at each time point time 0 was set to 100%.

Quantitative real-time RT-PCR

Total RNA was extracted using TRIzol reagent (Invitrogen) according to the manufacture's protocol. The first-strand cDNA synthesis was performed with random primers using cDNA synthesis kit from Takara. The quantitative PCR (qRT-PCR) was performed in the Eppendorf Master Cycler RealPlex using SYBR Green Kit from Takara. Primer sequences used for real-time RT-PCR are listed in Table S3.

Comet assay

Cells were plated at a density of 2×10^5 cells/well in 6-well plate followed by treatment with treatment with 5 μM Doxorubicin or 5 μM Camptothecin (CPT) for 12 h. Cells were then trypsinized and analyzed for comet assay as described previously (40). Briefly, cells embedded in agarose on a glass slide were incubated with lysis buffer (2.5 M NaCl, 0.1 M EDTA, 10 mM Tris, 1% SDS, 1% (v/v) Triton X-100, pH-10) containing10% DMSO for overnight at 4 °C. Slides were then incubated with alkaline electrophoresis buffer (10 M NaOH and 200 mM EDTA, pH-13) for 30 min to allow the DNA to unwind. Subsequently, electrophoresis was carried out for 30 min at 300 mA. Slides were neutralized with 0.4 M Tris buffer PH-7.5 and then immersed in 70% ethanol for 5 min, air dried, and stained with ethidium bromide, and imaged Images

were captured using a fluorescence microscope (Leica Microsystems), and the length of Comet tail was measured by using Image J software.

Flow cytometry analysis

Mitochondrial membrane potential (ΔΨm) was detected by a fluorescent JC-1 dye. MCF7 cells transfected with vector control and FBXL20 for 36 h were then either treated with DMSO or 5 μm Camptothecin for 12 h. Cells were washed twice with PBS and resuspended in serum-free DMEM medium containing JC-1 dye (Santacruz, sc-364116) for 30 min at 37 °C and analysed by flow cytometry. The fluorescence emission shift from red to green was determined as a change in mitochondrial membrane potential.

Percentage of apoptotic cells was determined using Annexin-V/7AAD staining kit (Biolegend). MCF7 cells expressing NS or FBXL20 shRNA or PUMA shRNA or BAX shRNA were treated with either DMSO or Doxorubicin 5 μM, 16 h. Cells were collected, washed with PBS/0.1% BSA, and incubated with FITC-conjugated Annexin V and 7AAD. Stained cells were analyzed by flow cytometry.

BAX oligomerization

BAX oligomerization assay was performed as described previously (41). Briefly, cells were treated with 5 μM Doxorubicin for 12 h as indicated. Treated cells then incubated with 2 mM Dithiobis (succinimidyl propionate) [DSP] (PG-82081, Pierce) for 30 min at room temperature in nonreducing buffer. Excess cross-linker 2 mM Dithiobis was quenched by the addition of 20 mM M Tris/HCl (pH 7.5) for 15 min at room temperature for 15 min. Cells were then washed with PBS twice, and the samples were then solubilized in 0.5% Nonidet P40 lysis buffer without a reducing agent and centrifuged at 12,000*g* for 10 min. BAX was detected by immunoblotting with an anti-BAX antibody.

Ubiquitination assays

MCF7 cells were cotransfected with indicated plasmids. After 36 h of transfection, cells were treated with 10 μM MG132 for additional 8 h. Then, cells were collected, washed with cold PBS, and lysed to prepare protein extracts as described above. Protein extracts (600 μg per pull down) were incubated with indicated antibodies for overnight at 4 °C with gentle rocking under denaturing condition (0.1% SDS). Beads were washed with lysis buffer three times, and bound proteins were eluted by boiling with 1× laemmli buffer. The eluted proteins were resolved by SDS-PAGE and immunoblotted with respective antibodies.

For *in vitro* ubiquitination assays, HEK-293T cells were transfected with plasmids encoding. DDK-FBXL20 or DDK-ΔFBXL20. Forty eight hours posttransfection, DDK-FBXL20 and DDK-ΔFBXL20 were immunopurified from the whole cell extracts using anti FLAG M2 magnetic beads (Sigma). The immunopurified proteins were incubated with recombinant GST-BAX or GST-PUMA, 0.1 mM E1 (UBE1; Boston Biochem), 0.25 mM E2 (UBCH5A; Boston Biochem), and

2.5 μg/ml ubiquitin (Boston Biochem) in the presence or absence of recombinant active AKT1 (Sigma, #SRP0353). Ubiquitylation reactions were performed in assay buffer (10 mM Tris (pH 7.5), 100 mM NaCl, 5 mM MgCl2, 5 mM ATP, 1 mM DTT) for 2 h at 30 °C. The reactions were stopped with 2× laemmli buffer, resolved on SDS-PAGE gels, and analyzed by immunoblotting using anti-GST antibody.

GST pull-down assay

Recombinant proteins were expressed in *E. coli* BL21(DE3) strain (NEB). Recombinant GST-PUMA and His-FBXL20 were purified using Glutathione Sepharose (GE healthcare) and Ni-NTA agarose (Thermo Fisher) beads respectively. For *in vitro* interaction studies, 5 μg of purified His-FBXL20 and 5 μg of purified GST-PUMA or GST-BAX (Sigma, #SRP5166) were mixed in a buffer (50 mM Tris-HCl, pH 7.4, 150 mM NaCl, 0.5 mM EDTA, 1% glycerol, 0.5% NP-40, 1 mM DTT, 1× protease inhibitor cocktail). In total, 20 μl glutathione Sepharose beads was added to the mixture and incubated for 1 h at room temperature on a rotator. The glutathione Sepharose beads were washed four times with the assay buffer. After washing, beads were resuspended in 10 μl of 2× Lammli buffer and heated at 90 °C for 5 min. The eluted proteins were immunoblotted with anti-His or anti-GST antibodies.

In vitro kinase assay

For *in vitro* kinase assay, His-FBXL20 truncations, His-FBXL20 (1–138aa), His-FBXL20 (135–240), His-FBXL20 (241–350aa), His-FBXL20 (350–435 aa) were purified from *E. coli* BL21(DE3) strain (NEB) using Ni-NTA agarose beads. GSK3α/β kinase was immunoprecipitated from HEK293T cell extracts using GSK3α/β antibody. Purified proteins were incubated with GSK3α/β kinase captured on beads in assay buffer (50 mM Tris-HCl at pH 7.5, 10 mM MgCl2, 2 mM DTT, 0.1 mM sodium orthovanadate and 0.1 mM EDTA 100 μM ATP) at 37 °C for 1 h. Reaction mixtures were then subjected to SDS-PAGE and immunoblotted with anti-phospho-serine and anti-phospho-threonine antibodies.

Tumor growth and mouse xenograft study

Animal experiments were performed in accordance with the guidelines of Institutional Animal Care and Ethics committee (IACEC) and approved by IACEC. For mouse xenograft MDAMB231 (5×10^6) cells expressing NS or FBXL20 shRNA were suspended in 1:1 PBS and Matrigel (1:1) and subcutaneously injected into the right flank of NOD-SCID mice. Tumor dimensions were measured every 3 days, and tumor volume was calculated using the formula $\pi/6 \times$ (length) × (width)^2.

Immunohistochemistry (IHC)

Our studies abide by the Declaration of Helsinki principles. The paraffin-embedded breast cancer patient tissue samples were obtained from SDM College of Medical Sciences, as per established core procedures and Institutional Ethical Board approval. Tissue samples were stained with hematoxylin–eosin to determine the histological type and grade of tumors. FBXO31, FBXL20, and PUMA protein levels in breast cancer patients, which include cancerous tissue and adjacent nonmalignant epithelium, were detected using immunohisto-chemical staining according to the method previously described ([42](#)). In brief, after deparaffinization and endogenous peroxidase blockage, the sections were heated in 0.01 M citrate buffer solution (pH 6.0) in water bath at 98 °C for 20 min, then incubated with the monoclonal antibody to PUMA (CST), BAX (CST), FBXO31(Sigma), and FBXL20 (Origene) at 1:100 dilution overnight at 4 °C, and visualized using 3,3′-diaminobenzidine (DAB) detection kit (Vector labs). For the negative control, anti-rabbit and anti-mouse IgG whole molecule (Sigma– Aldrich) was used at 1:1000 dilution. IHC stained samples were evaluated by two pathologists, and all samples were blinded. Staining intensity of these proteins in neoplastic cells was graded on a scale of 0 (no staining) to 3+ (strong staining). The protein expression was scored based on the percentage of positive cells: score 0 = 0% of stained positive cells; score 1 = weakly stained tissue or 1 to 25% of positive cells; score 2 = moderate stained tissue or 26 to 50% of positive stained cells; and score 3 = strongly stained tissue or more than 50% of stained cells.

Statistical analysis

All quantitative data were collected from at least three independent experiments and represented as mean ± SD. Difference between groups was determined using Student's *t* test using Microsoft Excel. p values <0.05 were considered significant.

Data availability

All data presented in the paper are contained within the article.

Posttranslational regulation of proapoptotic PUMA and BAX

References

1. Elmore, S. (2007) Apoptosis: A review of programmed cell death. *Toxicol. Pathol.* **35**, 495–516
2. Shimizu, S., Narita, M., and Tsujimoto, Y. (1999) Bcl-2 family proteins regulate the release of apoptogenic cytochrome c by the mitochondrial channel VDAC. *Nature* **399**, 483–487
3. Gross, A., McDonnell, J. M., and Korsmeyer, S. J. (1999) BCL-2 family members and the mitochondria in apoptosis. *Genes Dev.* **13**, 1899–1911
4. Cory, S., and Adams, J. M. (2002) The Bcl2 family: Regulators of the cellular life-or-death switch. *Nat. Rev. Cancer* **2**, 647–656
5. Yu, J., and Zhang, L. (2008) PUMA, a potent killer with or without p53. *Oncogene* **27**, S71–S83
6. Willis, S. N., and Adams, J. M. (2005) Life in the balance: How BH3-only proteins induce apoptosis. *Curr. Opin. Cell Biol.* **17**, 617–625
7. Jürgensmeier, J. M., Xie, Z., Deveraux, Q., Ellerby, L., Bredesen, D., and Reed, J. C. (1998) Bax directly induces release of cytochrome c from isolated mitochondria. *Proc. Natl. Acad. Sci. U. S. A.* **95**, 4997–5002
8. Zhang, M., Zheng, J., Nussinov, R., and Ma, B. (2017) Release of cytochrome C from Bax pores at the mitochondrial membrane. *Sci. Rep.* **7**, 2635
9. Narita, M., Shimizu, S., Ito, T., Chittenden, T., Lutz, R. J., Matsuda, H., and Tsujimoto, Y. (1998) Bax interacts with the permeability transition pore to induce permeability transition and cytochrome c release in isolated mitochondria. *Proc. Natl. Acad. Sci. U. S. A.* **95**, 14681–14686
10. Yu, J., Zhang, L., Hwang, P. M., Kinzler, K. W., and Vogelstein, B. (2001) PUMA induces the rapid apoptosis of colorectal cancer cells. *Mol. Cell* **7**, 673–682
11. Nakano, K., and Vousden, K. H. (2001) PUMA, a novel pro-apoptotic gene, is induced by p53. *Mol. Cell* **7**, 683–694
12. Chipuk, J. E., Kuwana, T., Bouchier-Hayes, L., Droin, N. M., Newmeyer, D. D., Schuler, M., and Green, D. R. (2004) Direct activation of Bax by p53 mediates mitochondrial membrane permeabilization and apoptosis. *Science* **303**, 1010–1014
13. Melino, G., Bernassola, F., Ranalli, M., Yee, K., Zong, W. X., Corazzari, M., Knight, R. A., Green, D. R., Thompson, C., and Vousden, K. H. (2004) p73 Induces apoptosis *via* PUMA transactivation and Bax mitochondrial translocation. *J. Biol. Chem.* **279**, 8076–8083
14. Ming, L., Sakaida, T., Yue, W., Jha, A., Zhang, L., and Yu, J. (2008) Sp1 and p73 activate PUMA following serum starvation. *Carcinogenesis* **29**, 1878–1884
15. Hershko, T., and Ginsberg, D. (2004) Up-regulation of Bcl-2 homology 3 (BH3)-only proteins by E2F1 mediates apoptosis. *J. Biol. Chem.* **279**, 8627–8634
16. You, H., Pellegrini, M., Tsuchihara, K., Yamamoto, K., Hacker, G., Erlacher, M., Villunger, A., and Mak, T. W. (2006) FOXO3a-dependent regulation of Puma in response to cytokine/growth factor withdrawal. *J. Exp. Med.* **203**, 1657–1663
17. Fricker, M., O'Prey, J., Tolkovsky, A. M., and Ryan, K. M. (2010) Phosphorylation of Puma modulates its apoptotic function by regulating protein stability. *Cell Death Dis.* **1**, e59
18. Sandow, J. J., Jabbour, A. M., Condina, M. R., Daunt, C. P., Stomski, F. C., Green, B. D., Riffkin, C. D., Hoffmann, P., Guthridge, M. A., Silke, J., Lopez, A. F., and Ekert, P. G. (2012) Cytokine receptor signaling activates an IKK-dependent phosphorylation of PUMA to prevent cell death. *Cell Death Differ.* **19**, 633–641
19. Proto-Siqueira, R., Panepucci, R. A., Careta, F. P., Lee, A., Clear, A., Morris, K., Owen, C., Rizzatti, E. G., Silva, W. A., Jr., Falção, R. P., Zago, M. A., and Gribben, J. G. (2008) SAGE analysis demonstrates increased expression of TOSO contributing to Fas-mediated resistance in CLL. *Blood* **112**, 394–397
20. Li, B., and Dou, Q. P. (2000) Bax degradation by the ubiquitin/proteasome-dependent pathway: Involvement in tumor survival and progression. *Proc. Natl. Acad. Sci. U. S. A.* **97**, 3850–3855
21. Lee, J. U., Hosotani, R., Wada, M., Doi, R., Kosiba, T., Fujimoto, K., Miyamoto, Y., Tsuji, S., Nakajima, S., Nishimura, Y., and Imamura, M. (1999) Role of Bcl-2 family proteins (Bax, Bcl-2 and Bcl-X) on cellular susceptibility to radiation in pancreatic cancer cells. *Eur. J. Cancer* **35**, 1374–1380
22. Nakayama, K. I., and Nakayama, K. (2006) Ubiquitin ligases: Cell-cycle control and cancer. *Nat. Rev. Cancer* **6**, 369–381
23. Jin, J., Cardozo, T., Lovering, R. C., Elledge, S. J., Pagano, M., and Harper, J. W. (2004) Systematic analysis and nomenclature of mammalian F-box proteins. *Genes Dev.* **8**, 2573–2580
24. Yu, J., Wang, Z., Kinzler, K. W., Vogelstein, B., and Zhang, L. (2003) PUMA mediates the apoptotic response to p53 in colorectal cancer cells. *Proc. Natl. Acad. Sci. U. S. A.* **100**, 1931–1936
25. Ciechanover, A. (1998) The ubiquitin-proteasome pathway: On protein death and cell life. *EMBO J.* **17**, 7151–7160
26. Jacobson, A. D., Zhang, N. Y., Xu, P., Han, K. J., Noone, S., Peng, J., and Liu, C. W. (2009) The lysine 48 and lysine 63 ubiquitin conjugates are processed differently by the 26 s proteasome. *J. Biol. Chem.* **284**, 35485–35494
27. Gardai, S. J., Hildeman, D. A., Frankel, S. K., Whitlock, B. B., Frasch, S. C., Borregaard, N., Marrack, P., Brattonm, D. L., and Henson, P. M. (2004) Phosphorylation of Bax Ser184 by Akt regulates its activity and apoptosis in neutrophils. *J. Biol. Chem.* **279**, 21085–21095
28. Ambacher, K. K., Pitzul, K. B., Karajgikar, M., Hamilton, A., Ferguson, S. S., and Cregan, S. P. (2012) The JNK- and AKT/GSK3β- signaling pathways converge to regulate Puma induction and neuronal apoptosis induced by trophic factor deprivation. *PLoS One* **7**, e46885
29. Choppara, S., Malonia, S. K., Sankaran, G., Green, M. R., and Santra, M. K. (2018) Degradation of FBXO31 by APC/C is regulated by AKT- and ATM-mediated phosphorylation. *Proc. Natl. Acad. Sci. U. S. A.* **115**, 998–1003
30. Yao, R., and Cooper, G. M. (1995) Requirement for phosphatidylinositol-3 kinase in the prevention of apoptosis by nerve growth factor. *Science* **267**, 2003–2006
31. Franke, T. F., Kaplan, D. R., and Cantley, L. C. (1997) PI3K: Downstream AKTi on blocks apoptosis. *Cell* **88**, 435–437
32. Zhu, J., Li, K., Dong, L., and Chen, Y. (2012) Role of FBXL20 in human colorectal adenocarcinoma. *Oncol. Rep.* **28**, 2290–2298
33. Zhu, J., Deng, S., Duan, J., Xie, X., Xu, S., Ran, M., Dai, X., Pu, Y., and Zhang, X. (2014) FBXL20 acts as an invasion inducer and mediates E-cadherin in colorectal adenocarcinoma. *Oncol. Lett.* **7**, 2185–2191
34. Downward, J. (1998) Mechanisms and consequences of activation of protein kinase B/Akt. *Curr. Opin. Cell Biol.* **10**, 262–267
35. Chen, W. S., Xu, P. Z., Gottlob, K., Chen, M. L., Sokol, K., Shiyanova, T., Roninson, I., Weng, W., Suzuki, R., Tobe, K., Kadowaki, T., and Hay, N. (2001) Growth retardation and increased apoptosis in mice with homozygous disruption of the Akt1 gene. *Genes Dev.* **15**, 2203–2208
36. Linseman, D. A., Butts, B. D., Precht, T. A., Phelps, R. A., Le, S. S., Laessig, T. A., Bouchard, R. J., Florez-McClure, M. L., and Heidenreich, K. A. (2004) Glycogen synthase kinase-3beta phosphorylates Bax and promotes its mitochondrial localization during neuronal apoptosis. *J. Neurosci.* **24**, 9993–10002
37. Hoeflich, K. P., Luo, J., Rubie, E. A., Tsao, M. S., Jin, O., and Woodgett, J. R. (2000) Requirement for glycogen synthase kinase-3beta in cell survival and NF-kappa B activation. *Nature* **406**, 86–90
38. Pap, M., and Cooper, G. M. (1998) Role of glycogen synthase kinase-3 in the phosphatidylinositol 3-kinase/Akt cell survival pathway. *J. Biol. Chem.* **273**, 19929–19932

39. Bradford, M. M. (1976) A rapid and sensitive method for the quantitation of microgram quantities of protein utilizing the principle of protein-dye binding. *Anal. Biochem.* **72**, 248–254

40. Olive, P. L., and Banáth, J. P. (2006) The comet assay: A method to measure DNA damage in individual cells. *Nat. Protoc.* **1**, 23–29

41. Nie, C., Tian, C., Zhao, L., Petit, P. X., Mehrpour, M., and Chen, Q. (2008) Cysteine 62 of Bax is critical for its conformational activation and its proapoptotic activity in response to H2O2-induced apoptosis. *J. Biol. Chem.* **283**, 15359–15369

42. Shetty, P., Bargale, A., Patil, B. R., Mohan, R., Dinesh, U. S., Vishwanatha, J. K., Pramod, B. G., Vidya, S. P., and Amsavardani, T. S. (2016) Cell surface interaction of annexin A2 and galectin-3 modulates epidermal growth factor receptor signaling in Her-2 negative breastcancer cells. *Mol. Cell. Biochem.* **411**, 221–233